2026 IEEE/SICE International Symposium on System Integration (SII)
January 11-14, 2026. Cancún, México

Integrating a 3-Axis Tactile Sensor Array on AIREC Robot for Human-like Radial Pulse Measuring

Reem Almheiri[1,4], Yushi Wang[2], Tito Pradhono Tomo[2], Tamon Miyake[2], Simon Gormuzov[1], Shigeki Sugano[3]

***Abstract*— Radial pulse measurement is an important physiological assessment method in healthcare and wellness monitoring. While most existing pulse measuring devices are dedicated instruments requiring precise placement, this work explores a human-like approach using a general-purpose humanoid robot. In this work, we present a proof-of-concept study on radial pulse measurement using the AIREC humanoid robot equipped with a 3-axis 8×6 matrix uSkin tactile sensor embedded in its palm. A dual-arm motion strategy allows one hand to support the subject's wrist while the other applies gentle pressure for stable human-robot contact. Contact stability is evaluated by both normal and shear measurements. Then, the tactile signals from the array are scanned to identify the optimal sensing location, and bandpass filtering is applied to extract the pulse waveform. Preliminary results show accurate pulse rate estimation compared with a commercial pulse oximeter, demonstrating the feasibility of a human-like bio-information measurement in humanoid robots.**

***Keywords*—human-robot interaction, tactile sensing, humanoid robot, dual-arm manipulation, radial pulse detection.**

I. Introduction

Rapid population ageing is reshaping care needs worldwide and acutely in Japan, where people aged older than 65 already comprise up to 29% of the population, intensifying demand for assistance in homes and care facilities [1]. General-purpose humanoid robots are a promising way to support diverse daily tasks in such settings, complementing limited human caregivers [2]. User acceptance is critical: robots that look and behave more like humans tend to elicit greater trust, social engagement, and compliance. Prior human-robot interaction (HRI) work shows that human-like form factors and socially engaging behaviors increase users' willingness to interact and be influenced, suggesting human-like interaction styles can smooth adoption in everyday contexts [3][4].

Among the many modalities of human-like interactions, physical touch remains relatively less explored in HRI than speech or vision. Physical touch interaction is often involved in human-assistance tasks [5][6][7]. Touch is distinctive as it has the ability to combine function with social meaning. Touch interaction is especially crucial for humanoid robots designed for caregiving, where touch can convey trust and emotional connection. Radial pulse assessment is a routine healthcare task, where caregivers can collect physiological data through gentle wrist palpation while offering reassurance. Pulse measurement is foundational in healthcare and wellness monitoring, with applications ranging from clinical triage to consumer wearables and remote patient monitoring. Reviews of non-invasive radial pulse sensing and large cohort studies highlight robust pulse-based monitoring in daily life [8][9][10].

Fig. 1. The humanoid robot AIREC measures the radial pulse at the human wrist via a tactile sensor embedded in its palm. During measurement, one hand supports the human wrist, while the other gently applies pressure to stabilize it.

However, introducing dedicated medical devices to home interactions can "medicalize" the encounter and reduce naturalness. In contrast, human clinicians often assess the radial pulse through gentle palpation with the fingers while supporting the wrist: an everyday, low-intrusion practice that people intuitively understand and thereby trust [11][12]. Beyond its functional role, touch itself carries social meaning: affectionate or caring touch regulates stress, supports attachment, and conveys emotion. Analogous touch-based cues have been explored in HRI as a channel for affect. Enabling robots to take a pulse via gentle touch could therefore preserve intimacy and acceptance while gathering biosignals [13][14]

Building on the importance of socially meaningful touch in caregiving, we utilized a dual-arm robot, AIREC [15], as our research platform. The robot is capable of gentle physical interaction, making it well-suited for exploring tactile sensing in physiological assessments. This paper proposes a human-like pulse-taking workflow on AIREC (shown in Figure 1)

*This work was supported by JST Moonshot R&D, Grant No. JPMJMS2031, and the Future Robotics Organization, Waseda University. Reem Almheiri also acknowledges the support of the Technology Innovation Institute (TII), Abu Dhabi, United Arab Emirates, which provides her financial support to conduct her study at Waseda University.

[1],Reem Almheiri and Simon Gormuzov are with Waseda University, Graduate School of Creative Science and Engineering, Tokyo, Japan. (Corresponding author: Reem Almheiri, e-mail: reem.almheiri@toki.waseda.jp)

[2]Yushi Wang, Tito Pradhono Tomo, and Tamon Miyake are with the Future Robotics Organization, Waseda University, Tokyo, Japan.

[3] Shigeki Sugano is with the Faculty of Science and Engineering, Waseda University, Tokyo, Japan.

[4]Reem Almheiri is also with Technology Innovation Institute (TII), Abu Dhabi, United Arab Emirates.

addressing the following challenges:

- Integration of tactile sensing: Seamless interation of 3-axis 8×6 uSkin tactile array in the robot's palm, enabling pulse measurement with rough wrist placement, while contact stability is ensured by jointly evaluating normal and shear forces to detect slip.
- Human-aware motion planning: An impedance-controlled dual-arm motion planning framework is developed, leveraging skeleton recognition to support and stabilize the human wrist during pulse measurement.
- Tactile signal processing: Implementing contact and slip evaluation, band-pass filtering, noise suppression, and array scanning for pulse-rate estimation.

These objectives form a proof-of-concept that aligns with everyday human practice while moving toward natural, acceptable robot-mediated pulse sensing in home settings.

The remainder of this paper is organized as follows. Section II presents a review of related work. The proposed method is then introduced in Section III. Section IV describes the experiments and their results. Finally, future work is provided in Section V.

II. Related Work

A. Robotic Palpation and Tactile Sensing

Robotic systems for pulse acquisition have been developed to automate palpation while ensuring consistent pressure and positioning. Notable examples include pulse-sensing robotic hands designed for tactile pulse palpation [16], multi-fingered robotic platforms for TCM pulse diagnosis [17], and robotic palpation systems capable of acquiring pulse waveforms for diagnostic purposes [18]. Reviews of tactile sensor systems for robotic palpation highlight the diversity of sensing technologies—from resistive and capacitive arrays to optical and magnetic methods—each with trade-offs in spatial resolution, sensitivity, and mechanical compliance [19]. Moreover, the above-mentioned method relied solely on a single-axis tactile sensor, thereby not accounting for the valuable information contained in shear forces regarding slip conditions.

Apart from healthcare, research has examined approaches that integrate tactile sensing into broader interactive contexts [20], such as social touch in assistive robots [21]. These works demonstrate that tactile interaction can serve not only as a diagnostic channel but also as a medium for building trust and emotional rapport, supporting the case for embedding pulse measurement within human-like behaviors of humanoid robots.

B. Touch-based Radial Pulse Sensing

Pulse measurement using tactile sensing is capable of capturing physiological signals without relying on dedicated medical devices [22]. Robotic systems have been developed to replicate the palpation techniques [23], including those inspired by Traditional Chinese Medicine (TCM) practices [24], [25]. Instrumentation developments include array-based pulse acquisition systems [26], [27] and prototypes

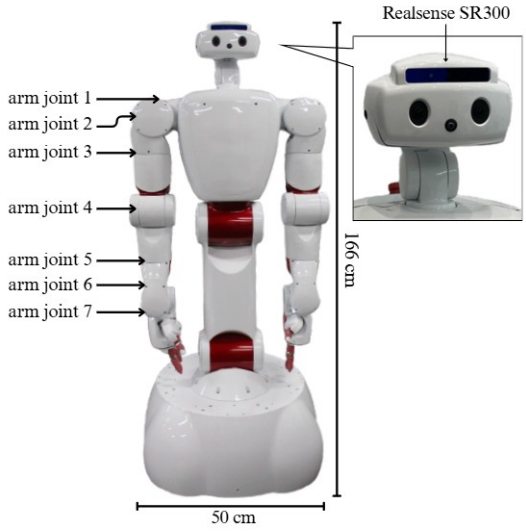

Fig. 2. Full-body view of the dual-arm humanoid robot AIREC and a close-up of the head showing the RGB-D camera.

capable of capturing both 3D pulse contour images and 1D pulse waveforms [28]. These advances are particularly valuable for accommodating variations in wrist placement and contact force.

Wearable sensors, such as wristbands, chest straps, and smartwatches, allow for continuous and mobile health monitoring [29], but prolonged skin contact can cause discomfort and their sensing is typically limited to a fixed body location. Non-contact optical methods, such as camera-based remote PPG (rPPG), detect subtle skin color changes caused by blood perfusion to estimate pulse rate [30], yet they are sensitive to lighting conditions, skin pigmentation, and movement, which can limit their robustness. In contrast, touch-based robotic systems can combine functional pulse measurement with human-like, reassuring interactions [3], [4].

There is a need for a robotic palpation method based on tactile sensing that operates in a human-like manner and does not require precise alignment between the human wrist and the sensor.

III. Methods

As previously mentioned, the AIREC robot shown in Figure 2 was used as our research platform. The robot consists of dual arms with hands, a torso, and an omnidirectional mobile base. All joints in the arms and torso are equipped with torque sensors, allowing position, velocity, and impedance control. The robot's head includes a RealSense SR300 RGB-D camera, which provides color and depth information. To enable a humanoid robot to perform human-like, natural pulse palpation, an array of tactile sensors is employed. The sensors are arranged in a matrix configuration, providing a sufficiently large sensing area so that precise positioning of the contact point is not strictly required. In typical clinical practice, pulse palpation is conducted for at least four seconds to ensure an accurate reading. To maintain stable measurements during this period, a dual-arm robotic configuration is adopted: one arm supports the subject's

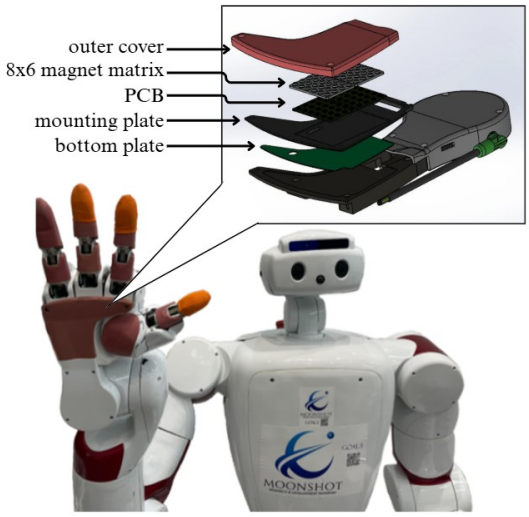

Fig. 3. AIREC robot showing tactile sensor location with exploded view of sensor assembly.

wrist, serving as the primary measurement platform, while the other arm gently applies pressure to the wrist to minimize unintentional movement, as seen in Figure 1.

A. Integration of uSkin sensor

In this work, a 3-axis tactile sensor is required: the normal force is used for pulse rate measurement, while the shear information together with the normal force is used to evaluate contact stability. Several soft tactile sensors capable of measuring 3-axis forces have been reported [31], [32]. For installation on a robotic hand, uSkin [33] was selected due to its ease of integration. The AIREC robot was originally equipped with elastomer coverings on its palms, so we embed uSkin sensor into the elastomer. This sensor comprises two uSPa46 modules arranged side-by-side, yielding a total of 48 taxels in an 8×6 matrix configuration. A custom outer cover was designed to eliminate any air cavity between the taxels and the sensing surface, mimicking the compliance of human soft tissue. The cover was fabricated via injection molding with a Shore hardness of 00-50. Its geometry follows the original AIREC Hand profile, maintaining the overall thickness, and incorporates a mounting base plate at the bottom to enable direct replacement of the original palm part (see Figure 3). Data acquisition is performed by two microcontrollers, each sampling the 24 taxels in three axes via I²C at 83 Hz per taxel. The microcontrollers are daisy-chained via a CAN bus, which is also used to transmit sensor data to the robot through a CAN–USB converter.

B. Algorithm Overview

The overall process can be described by a high-level control algorithm as seen in Figure 4. The flowchart outlines the stages that guide the robot through skeleton detection, subject interaction, and radial pulse data acquisition.

The algorithm begins with the robot transitioning from an initial home position to a predefined standby position. This standby position is an intermediate pose which provides a

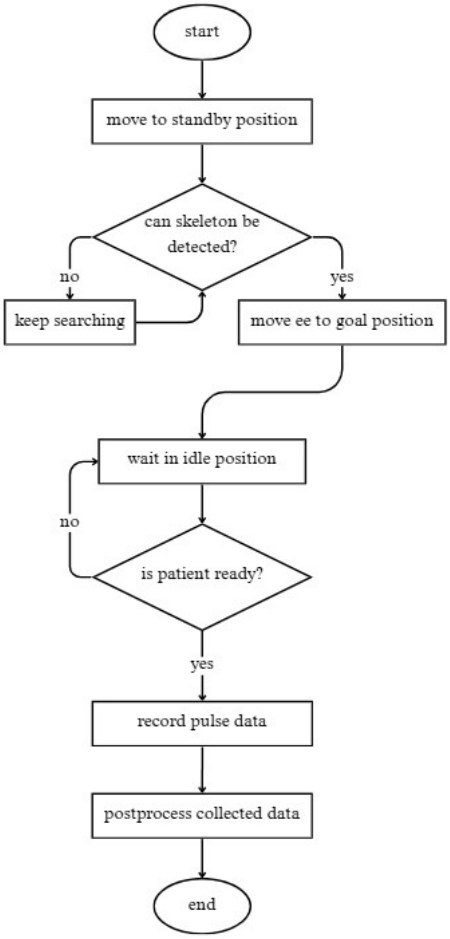

Fig. 4. Flowchart illustrating control flow of the proposed algorithm for radial pulse data acquisition.

consistent starting configuration regardless of subject variability. It also moves the robot head, and in effect, adjusts the camera angle to properly detect the human subject in the later stages. Once in standby, the algorithm initiates the MediaPipe [34] node, which uses Google's open-source framework for perception and image-processing, to detect the skeleton of the subject. If no skeleton is detected, the algorithm enters a loop, where it continuously searches until detection. If a skeleton is detected, then the algorithm moves the end-effector (denoted as ee) to a predefined goal with reference to the skeleton.

After the end-effector reaches the goal position, it transitions to an idle state. During the idle position, the robot waits for a manual confirmation by the operator that the subject is ready. The subject is required to rest their wrist on the robot's palm and remain as still as possible to be considered ready. To further ensure readiness, the algorithm monitors the wrist stability using the shear force information. If the subject is not ready, then the algorithm loops in the idle state and waits. Once the operator sends the confirmation signal, the robot begins the data acquisition process through the tactile sensor. This phase lasts approximately 15 seconds, after which the collected data undergoes a postprocessing step. The postprocessing may also be done offline as the data is

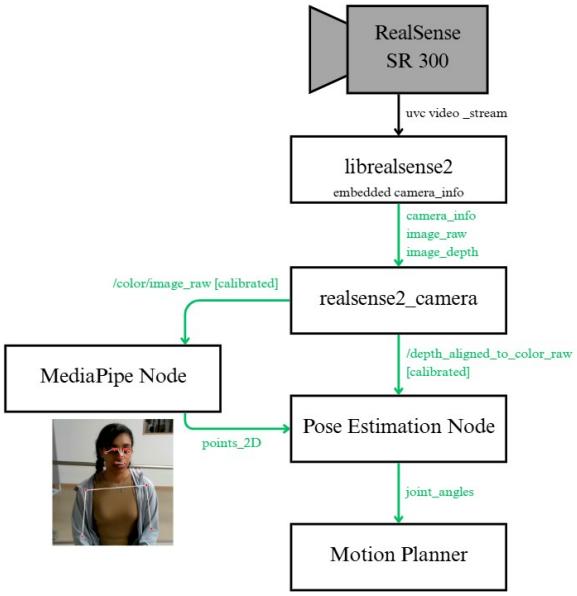

Fig. 5. Overview of the pipeline showing the RealSense SR300 video stream processing.

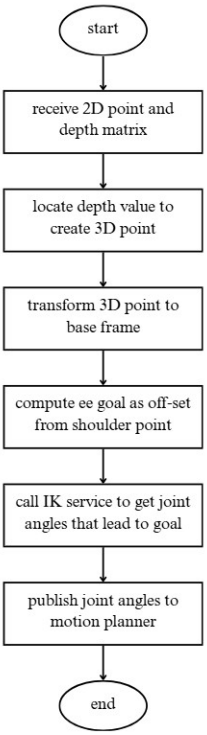

Fig. 6. Pose estimation node workflow from 2D and depth input to computing the end-effector goal.

also stored as comma-separated value files. Upon completion of the postprocessing stage, the algorithm terminates.

1) End effector position Estimation: To enable safe interaction with the subject, a vision system was utilized to guide the movement of the end-effector to a goal position relative to the detected subject's joint location. A RealSense SR300 RGB-D camera that captures both color and depth information was used. The overall processing pipeline is illustrated in Figure 5. The system subscribes to the `/color/image_raw` ROS topic published by the camera to receive the RGB image stream. These images are then processed through the *MediaPipe* node, which performs human pose estimation by detecting a set of predefined skeletal keypoints. For the purpose of this work, we focus specifically on the shoulder joint, since it provides essential relative position information between the robot and the human subject.

The *MediaPipe* node then passes the obtained 2D points to the *Pose Estimation* node (see Figure 6), which is also subscribed to the `/aligned_depth_to_color_raw` ROS topic published by the camera. This topic publishes a matrix consisting of per-pixel depth data aligned with the RGB image. Therefore, the corresponding depth value of the 2D points can be retrieved and a complete 3D point in the camera frame can be acquired, as seen in Figure 7.

The end-effector goal is therefore described relative from the detected shoulder point as:

$$EE^{\text{camera}} = P^{\text{camera}} + [x_{\text{off}}, y_{\text{off}}, z_{\text{off}}] \tag{1}$$

Where $x_{\text{off}}, y_{\text{off}}, z_{\text{off}}$ are predefined offset values that are chosen based on the desired spatial relation between the end-effector and the subject's shoulder. Specifically, x_{off} is zero in most cases, y_{off} is defined as half the shoulder length, and z_{off} is defined as half the distance between the robot and the subject.

Since the robot's control is conducted with reference to the base frame, the end-effector goal position is transformed using a static transform between the camera and the base $T^{\text{base}}_{\text{camera}}$ as:

$$EE^{\text{base}} = T^{\text{base}}_{\text{camera}} \cdot EE^{\text{camera}} \tag{2}$$

Finally, the end-effector goal is passed to a prebuilt inverse kinematics (IK) service, which converts the 3D Cartesian coordinates into the corresponding joint angles. These joint angles are then published to the robot's motion planner that plans and executes the trajectory needed to move the end-effector to the desired goal.

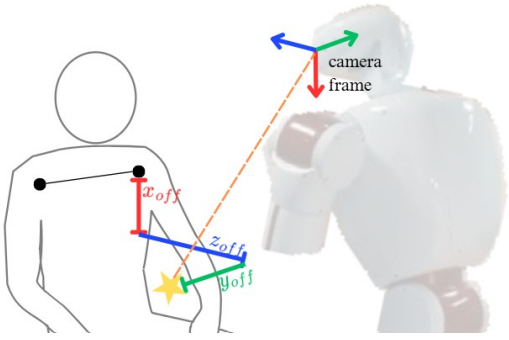

Fig. 7. Illustration depicting the relationship between the end-effector's goal (star) and the camera frame.

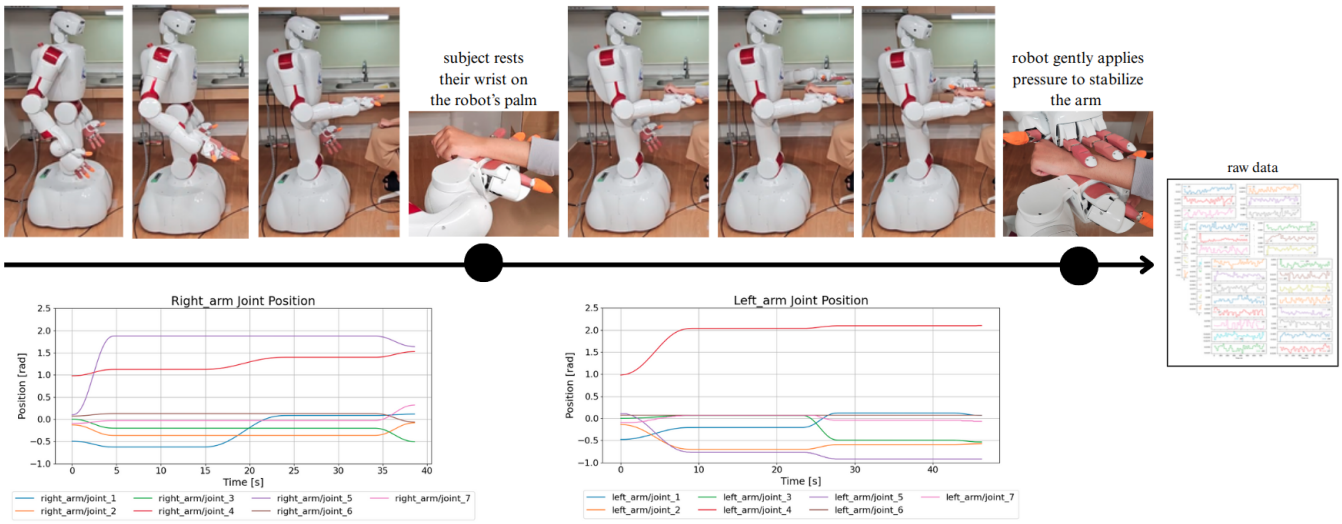

Fig. 8. AIREC robot's interaction with the subject during pulse measurement to produce raw tactile data for processing: (top) sequential images showing robot's motion and interaction with the subject, (bottom) corresponding joint angles of the robot's arms over time.

2) Pulse Measuring: To ensure reliable pulse acquisition, the onset of measurement was gated by a set of stability criteria derived from the tactile sensor array outputs. Specifically, the normal force measurement total was defined as

$$F_z = \sum_{i=1}^{N} f_{z,i}, \tag{3}$$

and the shear force total as

$$S_{\text{shear}} = \sum_{i=1}^{N} \sqrt{f_{x,i}^2 + f_{y,i}^2}, \tag{4}$$

where $f_{z,i}, f_{x,i}, f_{y,i}$ denote the three-axis readings of the i-th taxel, and $N = 48$ in the present setup.

Contact was assumed when the median normal force $\tilde{F}_z$ exceeded either (i) a baseline-referenced threshold

$$\tilde{F}_z > F_{z,\text{base}} + k_\sigma \, \text{IQR}(F_{z,\text{base}}), \tag{5}$$

with $k_\sigma = 1.2$, or (ii) a small absolute floor value $F_z > F_{z,\min}$ with $F_{z,\min} = 0.25$. The constant values were selected based on prior experiments, and IQR denotes the interquartile range of baseline fluctuations.

To monitor slip, the shear ratio was computed as

$$R_{\text{shear}} = \frac{S_{\text{shear}}}{F_z + \varepsilon}, \tag{6}$$

with $\varepsilon = 10^{-6}$ for numerical stability. A valid contact state required R_{shear} to remain below an adaptive limit

$$R_{\max} = r_{\text{base}} + 0.4 \cdot \frac{1}{1 + F_z}, \tag{7}$$

where r_{base} is set to be 1.8 based on successful measuring experience. Finally, to avoid false triggers from transient fluctuations, an additional dwell time of $T_{\text{dwell}} \approx 0.35\,\text{s}$ was required, such that all above conditions (contact, shear) had to be satisfied continuously for at least T_{dwell}. Once these criteria were met, the system automatically issued an *OK-to-measure* signal and proceeded to channel selection and pulse waveform extraction.

The tactile data produced 48 distinct channels corresponding to the x-, y-, and z-axis force components. For the purposes of pulse rate detection, only the z-axis channels were used, which represent the normal force. Each channel was processed with a two-stage Butterworth bandpass filter, first by a high-pass followed by low-pass. This is done in order to isolate the frequencies within the physiological range of radial pulses. The normal cutoff frequency ω_c was computed as:

$$\omega_c = \frac{f_c}{0.5 f_s} \tag{8}$$

where f_c is the cutoff frequency in hertz, and f_s is the sampling frequency, also in hertz. The selected range was determined from the relationship between the radial pulse in beats per minute (BPM) and frequency as:

$$f = \frac{\text{BPM}}{60} \tag{9}$$

This relation implies that 0.5 Hz corresponds to 30 BPM and 5.0 Hz corresponds to 300 BPM, which was the selected range. After filtering, each taxel signal was assigned a score that summarizes how reliable the signal is for pulse measurement. This quality score was computed as

$$\text{score} = \frac{\overline{p}}{\text{CV} + \varepsilon} \tag{10}$$

where $\overline{p}$ is the mean peak prominence, CV is the coefficient of variation of the peak intervals, and ε is a small constant to prevent division by zero. This metric favors signals that have well-defined peaks and are consistent in time. The signal with the highest score is selected, and the radial pulse in beats per minute is then computed as:

$$\text{BPM} = \frac{60}{\overline{\Delta t}} \tag{11}$$

where $\overline{\Delta t}$ is the mean time between successive peaks.

IV. Experiments and Results

During the experiments, the AIREC robot first uses its Realsense SR300 camera to detect the subject's skeleton with a few key points to estimate the position where it should reach out the hand. The subject then can place their wrist roughly on the robot's palm, thanks to the 6 x 8 arranged tactile sensor array, the radial artery on the wrist can be easily covered, even without precise guidance of a doctor. Then, the robot plans the motion of the left arm to press on the subject's wrist gently using an impedance controller, in this way to achieve safe interaction while also be able to keep the human wrist in place to eliminate unintentional movements that might cause pulse measuring artifacts. As seen in Figure 8. The motion planing performance was evaluated by comparing the actual joint positions to the desired. Across all joints of the right arm, the maximum deviation from the planned trajectory was 0.00065 ± 0.00064 rad, while the average deviation was 0.000034 ± 0.000019 rad. As for the left arm, the maximum deviation was 0.01367 ± 0.00964 rad, and the average deviation was 0.00707 ± 0.00557 rad. The increased variability in the left arm was considered to arise from the use of the impedance controller in conjunction with physical interaction with the subject's arm. The stabilizing pressure applied to the wrist may have perturbed the joints, thereby contributing to the observed variability.

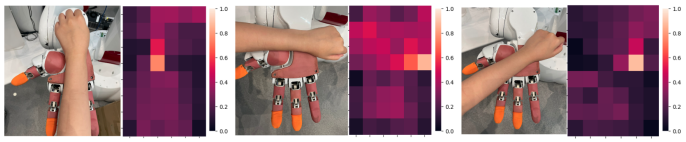

(a) (b) (c)

Fig. 9. Heatmaps showing sensor readings according to different wrist positions: (a) along the palm, (b) across the palm, and (c) diagonally.

Figure 9 shows the heatmaps of three wrist positions, this indicates a correct sensing in z-axis, as well as an acceptable spacial resolution of the tactile sensor. Figure 10 shows an example of filtered z - axis signals across all 48 taxels, and the selected signal according the the scoring criteria. By counting the periodic peaks within a certain period, we can measure a radial pulse rate.

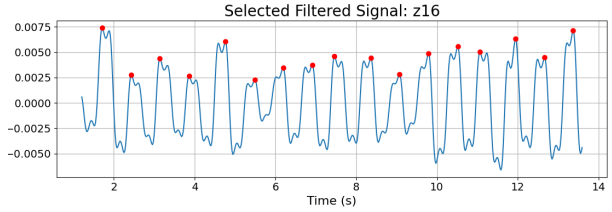

Fig. 10. Filtered z-axis data collected from 48 taxels and corresponding best signal according to the scoring criteria.

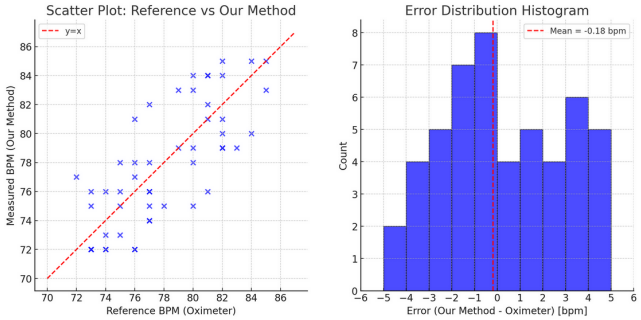

(a) (b)

Fig. 11. (a) Scatter plot of the pulse measuring results compared with an oximeter and (b) error distribution of the proposed method.

Fifty trials of pulse measurement were conducted using our dual-arm robotic tactile-sensor measuring method, with a commercial oximeter serving as the reference. Figure 11.a shows that the measurements from our method aligned closely with the oximeter values. Data points clustered around the diagonal, indicating strong agreement without obvious systematic over- or underestimation. However, some deviations are present and are mostly attributed to the difference in sensing modality as well as contact conditions while measuring. In Figure 11.b, the error distribution analysis showed that the majority of trials had small deviations from the oximeter reference, with errors centered around zero and a mean bias of approximately $+0.4$ BPM. Most measurements fell within ± 3 BPM, and the distribution was fairly symmetric. The standard deviation of 2.3 BPM further confirms that variability remained within acceptable limits, demonstrating both feasibility and consistency of the proposed approach.

V. Conclusions and Future Work

In this work, we propose a novel approach for integrating the uSkin tactile sensor array into the palm of the humanoid robot AIREC for radial pulse measurement. The incorporation of an 8×6 sensor matrix reduces the requirement for precise positioning of the radial artery, owing to its large coverage area and high resolution. To achieve human-like interaction and to mitigate fear associated with medical procedures, the robot is designed to use one arm to support the subject's wrist while the other arm gently presses on it to obtain more accurate measurements. The right arm employs a trajectory controller to provide stable wrist support, while the left arm applies an impedance controller to suppress motion artifacts from unintentional human movements, thereby ensuring both signal quality and safety. After contact stability is confirmed based on combined normal and shear force measurements, the processing algorithm filters and analyzes the signals from all 48 sensor channels to identify the most reliable waveform, from which the radial pulse rate is calculated.

Looking ahead, for enhanced human–robot interaction, a dialogue system will be introduced to explicitly guide the subject's actions, complemented by camera-based perception for improved mutual understanding and for substituting wrist

placement when necessary. Furthermore, beyond pulse rate estimation, the system aims to acquire clear pulse waveforms, which can provide richer information about cardiovascular health. Future work will also consider dynamic human movements during robot motion planning to ensure safer and more adaptive interaction. By exhibiting human-like palpation behaviors, the robot conveys care, trust, and reassurance through touch, thereby enriching the interaction beyond its functional role. In addition, the obtained pulse signals may be exploited in entertainment and interactive applications, such as adapting music, games, or storytelling to the participant's heartbeat. Finally, future work also includes evaluation of the proposed method in a social robotics context, examining how human-like tactile interactions influence user trust, comfort, and acceptance in both caregiving and everyday scenarios.

REFERENCES

[1] "https://www.who.int/news-room/fact-sheets/detail/ageing-and-health," accessed: 2025-08-15.

[2] "https://www.reuters.com/technology/artificial-intelligence/ai-robots-may-hold-key-nursing-japans-ageing-population-2025-02-28," accessed: 2025-08-15.

[3] V. Lu, J. Wirtz, and W. Kunz, "The role of the human-robot interaction in consumers' acceptance of humanoid retail service robots," *Service Industries Journal*, vol. 41, no. 13-14, pp. 924–947, 2021.

[4] J. Zonca, A. Folso, and A. Sciutti, "The role of reciprocity in human-robot social influence," *iScience*, vol. 24, no. 12, p. 103476, 2021.

[5] U. Yoo, N. Dennler, E. Xing, M. Matarić, S. Nikolaidis, J. Ichnowski, and J. Oh, "Soft and compliant contact-rich hair manipulation and care," in *2025 20th ACM/IEEE International Conference on Human-Robot Interaction (HRI)*. IEEE, 2025, pp. 610–619.

[6] T. Miyake, N. Saito, T. Ogata, Y. Wang, and S. Sugano, "Deep predictive learning with proprioceptive and visual attention for humanoid robot repositioning assistance," *2025 IEEE/RSJ International Conference on Intelligent Robots and Systems (IROS)*, 2025.

[7] M. Matsumura, T. Miyake, W. Choi, S. Sugano, K. Nakagawa, and E. Kobayashi, "Automated repositioning from supine to lateral with a humanoid robot based on body modeling," *2025 IEEE/RSJ International Conference on Intelligent Robots and Systems (IROS)*, 2025.

[8] B. Bent, B. A. Goldstein, W. A. Kibbe, and J. P. Dunn, "Investigating sources of inaccuracy in wearable optical heart rate sensors," *npj Digital Medicine*, vol. 3, p. 18, 2020, https://www.sciencedirect.com/science/article/pii/S2666389920301741.

[9] J. Parak and I. Korhonen, "Accuracy of firstbeat bodyguard 2 beat-to-beat heart rate monitor," *Sensors*, vol. 14, no. 12, pp. 23 493–23 505, 2014.

[10] A. Shcherbina, C. M. Mattsson, D. Waggott, H. Salisbury, J. W. Christle, T. Hastie, M. T. Wheeler, and E. A. Ashley, "Accuracy in wrist-worn, sensor-based measurements of heart rate and energy expenditure in a diverse cohort," *Journal of Personalized Medicine*, vol. 7, no. 2, p. 3, 2017, https://www.ncbi.nlm.nih.gov/pmc/articles/PMC5447130/.

[11] National Center for Biotechnology Information, "Pulse examination," https://www.ncbi.nlm.nih.gov/books/NBK470431/, accessed: 2025-08-15.

[12] Mayo Clinic, "How to check your pulse," https://www.mayoclinic.org/healthy-lifestyle/fitness/in-depth/pulse/art-20034334, accessed: 2025-08-15.

[13] M. J. Hertenstein, D. Keltner, B. App, B. Bulleit, and A. R. Jaskolka, "Touch communicates distinct emotions," *Emotion*, vol. 6, no. 3, pp. 528–533, 2006, https://www.tandfonline.com/doi/abs/10.1037/1528-3542.6.3.528.

[14] A. Gallace and C. Spence, "The science of interpersonal touch: An overview," *Neuroscience and Biobehavioral Reviews*, vol. 34, no. 2, pp. 246–259, 2010, https://www.ncbi.nlm.nih.gov/pmc/articles/PMC2866147/.

[15] T. Miyake, Y. Wang, P.-c. Yang, and S. Sugano, "Feasibility study on parameter adjustment for a humanoid using llm tailoring physical care," in *International Conference on Social Robotics*. Springer, 2023, pp. 230–243.

[16] Q. Peng, W. Zhang, Y. Yang, N. Li, and H. Liu, "A pulse-sensing robotic hand for tactile arterial palpation," in *2016 IEEE International Conference on Robotics and Biomimetics (ROBIO)*. IEEE, 2016, pp. 1922–1927.

[17] X. Zhang, L. Xu, J. Zhang, X. Wang, and W. Qiao, "Design of a robotic palpation system for standardized pulse diagnosis," *MATEC Web of Conferences*, vol. 218, p. 11024, 2018.

[18] Y. Wang and et al., "Robotic palpation for arterial pulse signal acquisition and analysis," *Procedia CIRP*, vol. 91, pp. 539–544, 2020.

[19] T. Matsui, T. Shibata, and et al., "Tactile sensor systems for robotic palpation: A review," *Applied Sciences*, vol. 12, no. 6, p. 2931, 2022.

[20] N. Gu, K. Kosuge, and M. Hayashibe, "Tactilealoha: Learning bimanual manipulation with tactile sensing," *IEEE Robotics and Automation Letters*, vol. PP, pp. 1–8, 01 2025.

[21] M. Konyo and S. Tadokoro, "Human-friendly palpation with a tactile sensor: From medical diagnosis to everyday assistance," *ACM Transactions on Human-Robot Interaction*, vol. 9, no. 3, pp. 1–20, 2020.

[22] W. Qiao, B. Xu, L. Xu, Q. Li, Z. Wang, and J. Wang, "The association of radial artery pulse wave variables with pulse diagnosis in traditional chinese medicine," *Evidence-Based Complementary and Alternative Medicine*, vol. 2018, pp. 1–10, 2018.

[23] Y. Li, P. Zhang, J. Wang, L. Xu, and W. Qiao, "Role of pulse diagnosis: A review," *Frontiers in Bioengineering and Biotechnology*, vol. 12, p. 1359297, 2024.

[24] L. Xu, Z. Wang, J. Wang, and W. Qiao, "How to standardize the pulse-taking method of traditional chinese medicine pulse diagnosis," *Frontiers in Bioscience*, vol. 26, no. 3, pp. 685–700, 2021.

[25] X. Zhang, L. Xu, J. Zhang, X. Wang, and W. Qiao, "Neural network study for standardizing pulse-taking depth by the width of artery," in *2018 3rd International Conference on Advances in Applied Science and Engineering (AASEC)*. EDP Sciences, 2018, p. 11024.

[26] Y. Bi, J. Li, W. Zhou, H. Zhang, X. Ma, and Z. Zhou, "Objective evaluation of pulse width using an array pulse diagram," *Biomedical Signal Processing and Control*, vol. 94, p. 106155, 2024.

[27] J. Zhang, L. Xu, X. Zhang, and X. Wang, "Comparison of sensors performance for the development of wrist pulse acquisition system," *Measurement*, vol. 59, pp. 273–282, 2015.

[28] J. Zhang, X. Zhang, X. Wang, and L. Xu, "Development and testing of a prototype for 3d radial pulse image measurement compatible with 1d pulse wave analysis," *Biomedical Signal Processing and Control*, vol. 31, pp. 214–221, 2017.

[29] J. Yin, P. He, H. Lv, Z. Zhang, X. Jiang, W. Chen, Y. Xu, and Q. Zheng, "A systematic review of non-invasive heart rate measurement using photoplethysmography," *Computers in Biology and Medicine*, vol. 124, p. 103955, 2020.

[30] Y. Bi, J. Li, W. Zhou, H. Zhang, X. Ma, and Z. Zhou, "Objective evaluation of pulse width using an array pulse diagram," *Biomedical Signal Processing and Control*, vol. 94, p. 106155, 2024.

[31] D. Abhyankar, Y. Wang, Y. Iwamoto, S. Sugano, and M. Kamezaki, "Development of permanent magnet elastomer-based tactile sensor with adjustable compliance and sensitivity," in *2024 IEEE/RSJ International Conference on Intelligent Robots and Systems (IROS)*, Abu Dhabi, United Arab Emirates, 2024, pp. 11 434–11 441.

[32] Y. Wang, M. Kamezaki, Q. Wang, H. Sakamoto, and S. Sugano, "3-axis force estimation of a soft skin sensor using permanent magnetic elastomer (pme) sheet with strong remanence," in *2022 IEEE/ASME International Conference on Advanced Intelligent Mechatronics (AIM)*, Sapporo, Japan, 2022, pp. 302–307.

[33] XELA Robotics, "Xela robotics – human-like tactile sensing for robots," https://www.xelarobotics.com/, accessed: 2025-08-14.

[34] C. Lugaresi, J. Tang, H. Nash, C. McClanahan, E. Uboweja, M. Hays, F. Zhang, C.-L. Chang, M. Yong, J. Lee, W.-T. Chang, and M. Grundmann, "Mediapipe: A framework for perceiving and processing reality," in *Proceedings of the 3rd Workshop on Computer Vision for AR/VR at IEEE Conference on Computer Vision and Pattern Recognition (CVPR)*, 2019, accessed: 2025-08-15. [Online]. Available: https://arxiv.org/abs/1906.08172